Microporous and Mesoporous Materials 231 (2016) 216–229

Contents lists available at ScienceDirect

Microporous and Mesoporous Materials

journal homepage: www.elsevier.com/locate/micromeso

Influences of the confinement effect and acid strength of zeolite on the mechanisms of Methanol-to-Olefins conversion over H-ZSM-5: A theoretical study of alkenes-based cycle

Wenna Zhang [a, c], Yueying Chu [b], Yingxu Wei [a], Xianfeng Yi [b, c], Shutao Xu [a], Jindou Huang [a], Mozhi Zhang [a, c], Anmin Zheng [b, **], Feng Deng [b], Zhongmin Liu [a, *]

[a] National Engineering Laboratory for Methanol to Olefins, Dalian National Laboratory for Clean Energy, iChEM (Collaborative Innovation Center of Chemistry for Energy Materials), Dalian Institute of Chemical Physics, Chinese Academy of Sciences, Dalian 116023, PR China
[b] State Key Laboratory of Magnetic Resonance and Atomic Molecular Physics, National Center for Magnetic Resonance in Wuhan, Institute of Physics and Mathematics, Chinese Academy of Sciences, Wuhan 430071, PR China
[c] University of Chinese Academy of Sciences, Beijing 100049, PR China

ARTICLE INFO

Article history:
Received 9 March 2016
Received in revised form
28 April 2016
Accepted 21 May 2016
Available online 24 May 2016

Keywords:
Methanol-to-Olefins conversion
Zeolite catalysts
Reaction mechanism
Confinement effect
Acid strength
Density functional theory

ABSTRACT

Methanol-to-Olefins (MTO) conversion over acidic zeolite catalysts has become the most important non-petrochemical route for the production of light olefins. The 'dual-cycle' mechanism (i.e., alkenes-based cycle and aromatics-based cycle) over H-ZSM-5 zeolite has been generally accepted for olefins generation from methanol conversion. However, the relationship between the catalytic performance and the confinement effect/acid strength of the catalyst is still unclear. Herein, the methylation, isomerization and cracking processes involved in the alkenes-based cycle are discussed in-depth by density functional theory (DFT) calculations. The calculation results predicted that the transition states can be considerably stabilized by the van der Waals (vdW) interactions from the zeolite framework, resulting in the reduction of the activation barriers. And acid strength can also enhance the reaction activities. However, the catalytic reactivity of all elementary steps in the alkenes-based cycle can be improved at a different degree with increasing the acid strength. In addition, the ethene formation, transformation and the precursor of ethene formation need higher energy. And increasing acid strength can sharply decrease the activation barriers of ethene formation of cracking reaction, indicating that ethene formation may need strong acid strength.

© 2016 Elsevier Inc. All rights reserved.

1. Introduction

With the increase of the global demand for energy and the petrochemical products and the growing depletion of oil resources, developing substitute resources has been the focus of petrochemical industry [1,2]. Methanol-to-Olefins (MTO) process is considered as the most important non-petrochemical route, which can convert the abundant resources such as coal, natural gas and biomass into light olefins [1](e.g., ethene and propene). Therefore, in order to understand the MTO process (improving reactivity, regulating the distribution of products), the fundamental study of the MTO reaction have attracted considerable attentions of many researchers since 1970s [3]. In the past decades, great efforts have been devoted to the catalytic mechanism of MTO reaction using experimental and theoretical methods, especially on the zeolite H-ZSM-5 and zeotype catalyst H-SAPO-34 as the two promising catalysts [4–7].

In the previous studies, researchers paid a lot of attentions to the direct mechanism that the formation of first C–C bond from C1 reactant derived from methanol or DME (Dimethyl Ether) in the MTO process [2]. More than 20 mechanisms have been proposed to explain the formation of first C–C bond with various reactive intermediates participation such as oxonium ylides [8a,b], carbocations [8c,d], carbenes [3] and free radicals [8e,f]. However, most of them have been energetically unfavorable due to the high barriers (>200 kJ/mol) [9–11]. Nowadays, the indirect mechanism, hydrocarbon pool mechanism, firstly described by Dahl and Kolboe over

* Corresponding author.
** Corresponding author.
E-mail addresses: zhenganm@wipm.ac.cn (A. Zheng), liuzm@dicp.ac.cn (Z. Liu).

http://dx.doi.org/10.1016/j.micromeso.2016.05.029
1387-1811/© 2016 Elsevier Inc. All rights reserved.

SAPO-34 [4,5,7] has been generally accepted and applied to explain various theoretical and experimental results. Then two distinct reaction routes of hydrocarbon pool mechanism have been proposed, named side-chain methylation route and paring route [12–14]. A further suggestion about 'dual-cycle' reaction for olefin generation from methanol conversion over H-ZSM-5 was made by the groups of Olsbye [15,16]. The ethene and propene are formed from the lower methylbenzenes via the aromatics-based cycle and the C_3^+ alkenes are formed through rapid olefin methylation and cracking steps (the alkenes-based cycle) [16].

Aromatics-based cycle (side-chain mechanism and paring mechanism) have been intensively studied [4,5,7,12–14,17], in which methylbenzenes are considered as the most important hydrocarbon pool species, but some issues still exist unsolved due to the difficulty in the observation of intermediates [18–22]. Recently, the role of alkenes on the MTO mechanism has also received great attention. Dessau has first proposed the olefin methylation and cracking route based on ^{13}C labeling experiments in a recently study [23,24]. Van Speybroeck et al. suggested a possible route for the production of propene and ethene in the 'alkenes-based cycle' over H-ZSM-5 [25]. And the research of Wang et al. indicated that olefins themselves other than hexamethylbenzene (MBs) are likely to be the dominating hydrocarbon pool species in H-SAPO-34 [26,27], H-SSZ-13 [28] and H-ZSM-5 [29]. Based on these studies, the olefin methylation and cracking route (alkenes-based cycle) plays an important role in the MTO mechanism. In this route (alkenes-based cycle, as shown in Scheme 1) higher olefins are formed through continuously methylation (**Me0-Me3**), and the formed carbenium ions and their isomers generated by isomerization (**I1-1-I3-2**) reactions can be cracked into the light olefins (**Cr1-1-Cr3-3**).

The confinement effect and acidity, as two important properties of zeolite catalysts, play a crucial role in the catalytic reactivity and the product selectivity of heterogeneous reaction over zeolite catalysts [30–35]. Many researchers have extensively explored the relationships between reactivity and zeolite properties (the framework confinement effect and acidity) by experimental and theoretical results [30–36]. The zeolite pore structures could strongly mediate the catalytic performance, hence, the confinement effect on the catalytic reaction has been investigated extensively [31,33]. It's illustrated by Waroquier et al. that the CHA cages provide the more perfect surroundings than Beta and H-ZSM-5 zeolites in the hexamethylbenzene methylation reaction [33] for heptamethylbenzeniumcation formation. Wang et al. discussed the influences of different zeolite framework topology (CHA, AEI and AFI) on MTO reactions [37]. Furthermore, an investigation has demonstrated that the zeolite confinement effect can affect the stabilities of the transition states on the alkenes dimerization reactions [31].

Besides the confinement effect, the acid strength can also strongly determine the reaction activities. It's demonstrated that the stronger Brønsted acid sites can significantly enhance the reactivity of the alkane activation [38], but dramatic decrease the reaction rates of the cyclohexanoneoxime Beckmann rearrangement reaction in the zeolite catalysts [39]. In order to explore the influence of acid strength on the MTH (Methanol to Hydrocarbon) reaction activity, H-ZSM-5 zeolites with varied acid strengths (H-[Al]-ZSM-5, H-[Fe]-ZSM-5, and H-[Al, Fe]-ZSM-5) were prepared,

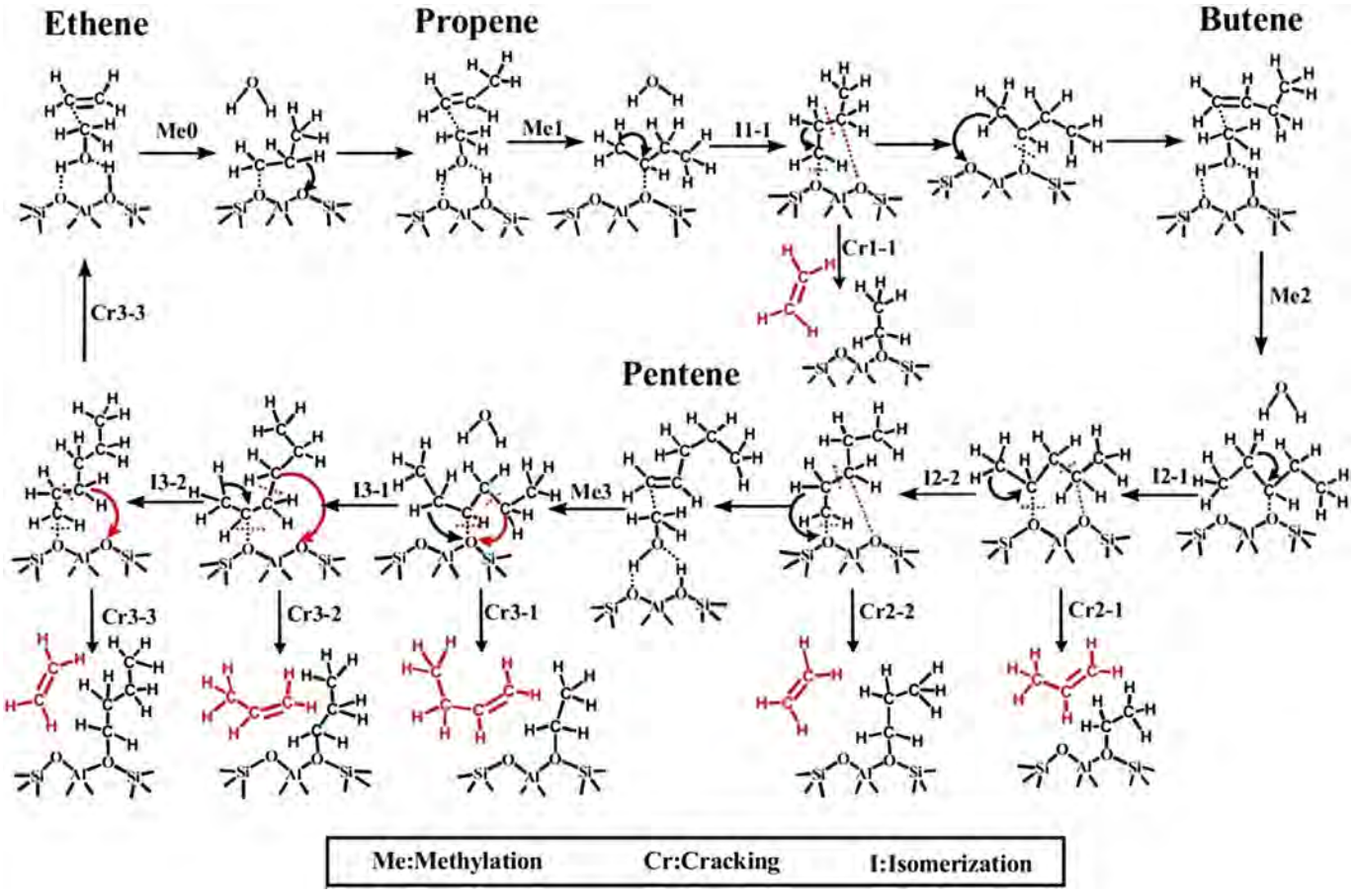

Scheme 1. Olefin methylation and cracking route of alkenes-based cycle for MTO conversion.

and catalytic test has suggested that the optimized H-[Al, Fe]-ZSM-5 with a broad acid strength distribution has the best catalytic performance and superior P/E (propylene/ethylene) ratio [30]. Zheng et al. studied the influence of Brønsted acid strength on the ethylene dimerization [31] and Beckmann rearrangement reaction [40] by density functional theory (DFT) calculations, illustrating theoretically that the acid strength will considerably determine the reaction mechanism and reactivity. In addition, it is confirmed that strong acid strength could significantly improve the selectivity of propene through the catalytic cracking of 1-butene on the P-modified and HNO_3-dealuminated H-ZSM-5 [32]. Therefore, a systematic investigation on the influences of the confinement effect and acid strength of zeolite are of great significance for regulating reaction process and clarifying the mechanism.

In this work, the influences of the confinement effect and the acid strength of zeolite catalysts in the alkenes-based cycle of MTO reaction have been investigated by the density functional theory (DFT) calculations. In DFT calculations, an 8T model representing the local structure of Brønsted acid site and an extended 72T model representing the complete framework structure of zeolite H-ZSM-5 were used to investigate the confinement effect of the zeolite frameworks. In order to demonstrate acid strength of the zeolite frameworks on the MTO reaction reactivity, Al-ZSM-5 and B-ZSM-5 of 72T models were used to illustrate the role of the acid strength. Our theoretical calculations were performed to correlate the catalytic performance to the confinement effect/acid strength of the zeolite catalyst in MTO reaction, which will be helpful in optimizing the reaction of methanol to olefins.

2. Calculation methods

It's demonstrated that the confinement effect from the zeolite pores structures have strong influence on the reaction process and catalytic performance [31,33]. Therefore, it is necessary to investigate the confinement effect on the reaction process from the zeolite framework theoretically. In this work, we used the extended 72T model to represent the H-ZSM-5 complete pore structure to estimate the confinement effect of the zeolite frameworks (see Fig. 1). And 8T model only contains the local properties of activation center, neglecting the space constraints and electrostatic effects derived from zeolite framework. In the calculations, 8T model of H-ZSM-5 was modeled as a cluster of stoichiometry $[(H_3SiO)_3{-}Si{-}OH{-}Al{-}(OSiH_3)_3]$, which was extracted from the crystalline structure of the H-ZSM-5 zeolite [41]. During the structure optimization of the 8T cluster model, the terminal hydrogen was fixed while the rest of atoms were relaxed. Therefore, these two models (see Fig. 1) were used to investigate the confinement effect of the zeolite frameworks on the reactions of alkenes-based cycle.

It's well known that the strengths of the Brønsted acid sites of isomorphously framework substituted H-ZSM-5 in accordance of the sequence of [B]-ZSM-5 < [Al]-ZSM-5 [29,35,42,43]. In this work, we used a H-ZSM-5 of 72T cluster model with different heteroatom B or Al to represent the environment with weak acidity or strong acidity (Fig. 1). The Al12–O24(H)–Si12 intersection site was used to represent the Brønsted acid site. Because this site is located in the intersection of the straight channel and the sinusoidal channel of zeolite H-ZSM-5 and it is easy access by adsorbents and has maximum reaction space [44,45]. All primary Si–H was fixed at a bond length of 1.47 Å, oriented along the direction of the corresponding Si–O bond. Therefore, Al-ZSM-5 and B-ZSM-5 of 72T model were used to investigate the influence of acid strength on the reactions of alkenes-based cycle in next section.

The combined theoretical model, namely, ONIOM (ωB97XD/6-31G(d,p):MNDO) was applied to predict the geometries of various adsorption structures and transition states, which was used on the calculation of zeolite catalyzing reactions widely [31,33,46]. The geometries were optimized using ωB97XD hybrid density function with 6-31G(d, p) basis sets, where the ωB97XD method is the hybrid meta DFT developed by Chai and Head-Gordon [47]. This method implicitly accounts for empirical dispersion and can describe long-range dispersion interactions well with respect to the traditional DFT methods. In the search of transition state structure, QST3 method was used to determine the transition state structure [48]. To preserve the integrity of the zeolite structure during the structure optimizations, only the $(SiO)_3{-}Si{-}OH{-}Al{-}(SiO)_3$ active center and the adsorbed species in the high-level layer were relaxed while the rest of atoms were fixed in the low-level at their crystallographic locations [29,40,49]. Then, the single-point energies were calculated at the level of ωB97XD/6-31G(d,p) [41]. The activation barrier is defined as the energy difference of the reactant and transition state in each reaction step. For the reactions catalyzed on the 8T model of H-ZSM-5, the frequency calculations were performed at the same level as geometry optimizations to check whether the saddle points exhibit the proper number of imaginary frequencies. Only a single imaginary frequency was observed for the transition state. The TS structure of 72T model can be confirmed from the trends of the mode for the cleavage and formation of the chemical bonds on the basis of the similarity of transition state structure of 8T model. The energies reported here have not been corrected for zero point vibration energies. The convergence criteria of max force, rms force, max displacement and rms displacement are 4.5×10^{-4}, 3.0×10^{-4}, 1.8×10^{-3} and 1.2×10^{-3}. All the geometry optimizations and frequency calculations were performed using the Gaussian 09 package.

To visualize the noncovalent interactions between the adsorbed organic species and the zeolite framework, the noncovalent interaction index approach, developed by Yang et al. [50], was adopted. In this approach, the reduced density gradient (RDG), defined as $RDG(r) = 1/(2(3\pi^2)^{(1/3)})\ |\nabla\rho(r)|/(\rho(r)^{(4/3)})$, together with the electron density ρ, was used to distinguish the covalent and noncovalent interactions. The noncovalent interactions are located at the regions with low density and low RDG. The sign of the second largest eigenvalue (λ2) of the electron density Hessian is helpful to distinguish bonded ($\lambda2 < 0$) from nonbonded ($\lambda2 > 0$) interactions. In addition, the sigh of λ2 can identify different types of noncovalent interactions: ($sign(\lambda2)\rho < 0$, H-bonding interaction; $sign(\lambda2)\rho \approx 0$, weak van der Waals (vdW) interaction and $sign(\lambda2)\rho > 0$, strong repulsive interaction). To reveal clearly the intermolecular noncovalent interaction between the adsorbed organic species and the zeolite framework, the intramolecular interactions are eliminated for the calculated RDG function. The functions RDG and $sign(\lambda2)\rho$ were calculated with the Multiwfn software [51].

3. Results and discussion

3.1. Effects of confinement effect on the methanol conversation following alkenes-based cycle

The previous works had demonstrated the alkenes-based cycle was a well-known alternative pathway for the MTO reaction [23,25–28,52]. As well known, the zeolite confinement effect and acidity play an important role on acid-catalyzed reactions [31,40,52]. In the following, the relationships between the confinement effect/acid strength and the alkenes-based MTO mechanisms (including methylation, isomerization and cracking reaction from C_2 to C_7) were discussed in detail. For exploring the influences of alkenes dimension on the MTO reactivity, six alkenes (ethene, propene, butene, pentene, hexene and heptene) were considered in the work.

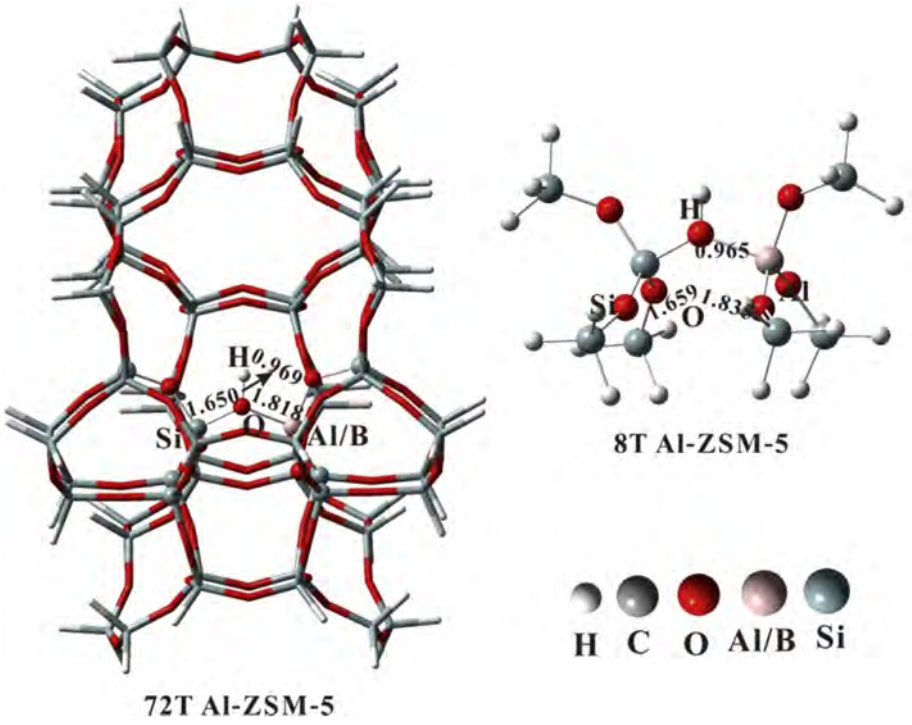

Fig. 1. Representations of H-ZSM-5 framework structures by 72T cluster models and the 8T H-ZSM-5 cluster model. The 8T cluster model in the extended cluster model represented as ball and stick view was treated as the high-layer atoms during the ONIOM calculations.

3.1.1. Olefin methylation

The effect of confinement effect of the catalyst on olefin methylation (as shown in Table 1) was determined by comparing the activation barriers of methylation for olefins on the acid site in the 8T model and 72T model with complete pore structure of zeolite. In order to further illustrate the methylation difference of different olefin size, the calculations of ethene, propene, butene, pentene, hexene and heptene methylation were involved (**Me0-Me5**, Table 1). Figs. 2 and 3 show the geometry of the transition states for the olefin methylation reaction on the H-ZSM-5 of 8T cluster model and 72T cluster model with complete pore structure of zeolite, and Table 1 provides the main geometrical parameters and activation barriers. The transition structure shows that the new C–C bond formation, accompanied by the methanol dehydration, forms the higher carbenium ion. Taking propene methylation on catalyzed on 8T Al-ZSM-5 for instance, the distance of C1–O3 (2.110 Å) illustrates that C1 atom on the methyl group moves away from O3 with the formation of new C1–C2 bond (2.167 Å) in the transition state (TS, Fig. 2b). In addition, the double bond of C2=C3 on propene is elongated from 1.332 Å in the adsorbed state to 1.354 Å in the transition state (TS, Fig. 2b), indicating that the C2=C3 double bond is converted into a single bond. Hence, the CH_3 group transfers to the olefin with methanol dehydration, and then butyl carbenium ion are produced. Similar to the olefin methylation on the 8T model described earlier, the structure of transition state on the 72T model is identified in which the adsorbed methanol dehydration leads to the formation of higher carbenium ion. When the propene methylation (**Me1**) occurs (Fig. 3b), the transition state structures indicated that the C1–O3 bond (2.020 Å) is broken together with migration of the CH_3 group from O3 to C2 (r_{C1-C2} = 2.233 Å) and lengthening the C2=C3 bond length to 1.352 Å (Fig. 3b).

It can be noted that the size of olefins slightly affects the structures of the transition states whether on the 8T model or on the 72T model (Figs. 2 and 3). For example, in the transition state structure of the ethene methylation (**Me0**, Fig. 2a) on 72T model with complete pore structure of zeolite, the longest distance of C1–C2 bond (2.250 Å) suggests that the C1 atom (methyl group) is difficult to transfer from O3 to C2. In contrast, for the transition states structures of the butene and other higher olefins in **Me2** to **Me5**, the bond distances of C1–C2 (2.223–2.239 Å) and C2=C3 (1.352–1.353 Å) are nearly identical in all cases. Consequently, and the activation barriers of ethene methylation (31.53 kcal/mol) is higher than other higher olefins methylation (**Me2-Me5**, *ca.* 25–27 kcal/mol). This result is consistent with the experimental study of Svelle that an intrinsic activation energy of ethene methylation(135 kJ/mol = 32.30 kcal/mol) [53] on H-ZSM-5 is higher than the propene (110 kJ/mol = 26.32 kcal) and n-butene(90 kJ/mol = 24.53 kcal/mol) [54] and their theoretical results [55]. In addition, the difference of olefin size were explored on H-SAPO-34 [26] and all the calculation energy of olefin methylation (1.54–1.83 ev/35.51–41.51 kcal/mol) were higher than our calculation (26–32 kcal/mol) for the weaker acidity of H-SAPO-34 zeolite. However, the same tendency were also determined on the H-SAPO-34 that the activation energy of ethene is as high as 1.83 ev

Table 1
Activation barriers (kcal/mol) and the main geometrical parameters (Å) of the transition-state for the olefin methylation on 8T Al-ZSM-5 cluster model and 72T Al-ZSM-5 cluster model: ethene (**Me0**), propene (**Me1**), butene (**Me2**), pentene (**Me3**), hexene (**Me4**) and heptene (**Me5**).

Reaction	Activation barrier		Geometry parameters (8T Al-ZSM-5)			Geometry parameters (72T Al-ZSM-5)		
	E_{8T}	E_{72T}	r_{C1-O3}	r_{C1-C2}	r_{C2-C3}	r_{C1-O3}	r_{C1-C2}	r_{C2-C3}
Me0	36.94	31.53	2.138	2.201	1.349	2.060	2.250	1.349
Me1	36.47	29.27	2.110	2.167	1.354	2.020	2.233	1.352
Me2	34.26	25.27	2.095	2.174	1.354	2.027	2.223	1.353
Me3	34.72	26.61	2.090	2.183	1.355	2.029	2.229	1.353
Me4	34.26	26.29	2.090	2.180	1.355	2.026	2.226	1.352
Me5	34.42	26.04	2.095	2.173	1.355	2.019	2.239	1.352

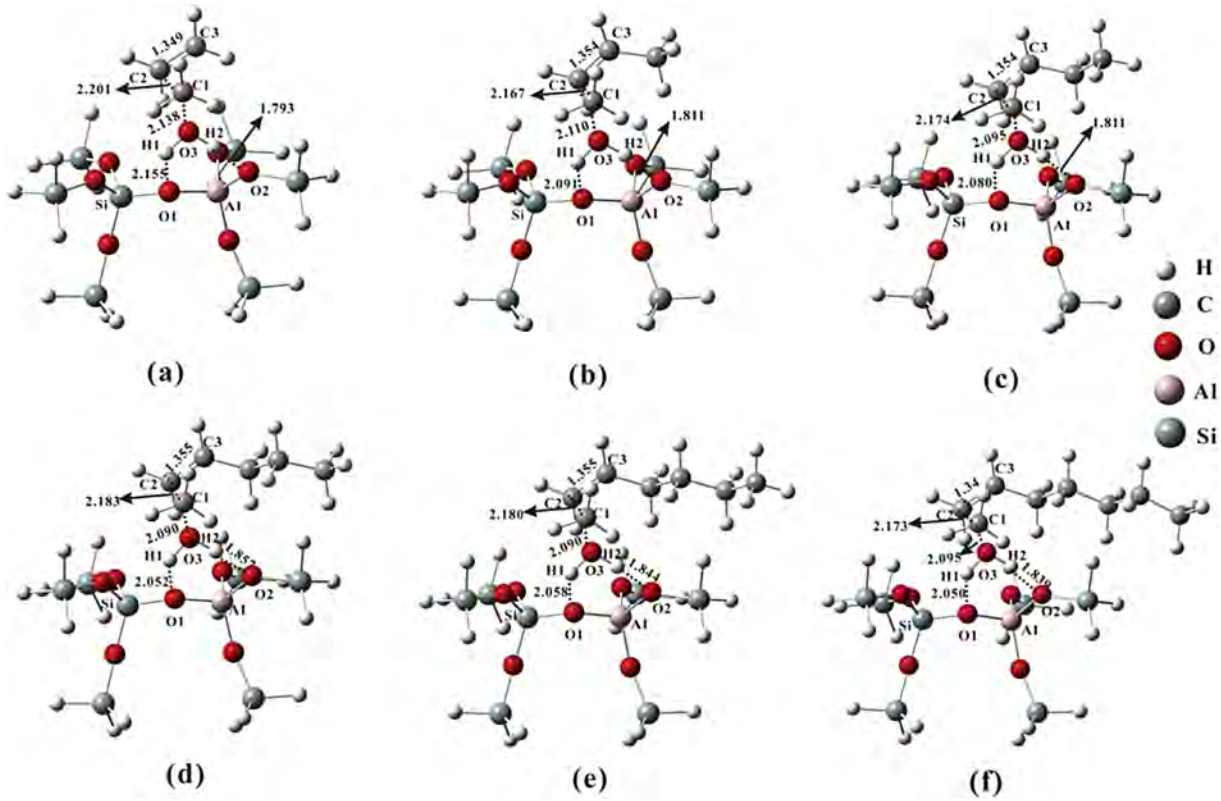

Fig. 2. Optimized geometries of the transition state (TS) for the olefin methylation on Al-ZSM-5 of 8T model: (a) ethene (**Me0**) (b) propene (**Me1**) (c) butene (**Me2**) (d) pentene (**Me3**) (e) hexene (**Me4**) (f) heptene (**Me5**). Selected bond distances (in Å) are indicated.

(41.51 kcal/mol) than other higher olefins (1.54–1.59 ev/ 35.51–36.67 kcal/mol) [26]. And the same result were obtained on other zeolite of FER, MOR, and BEA that lower activation barriers and higher rate constants for propene methylation were observed in comparison with ethene [56,57]. It is therefore confirmed that ethene methylation need to overcome higher activation barrier, which should be mainly ascribed to the formation of the unstable primary carbenium ion. With the increase of the olefin size, the

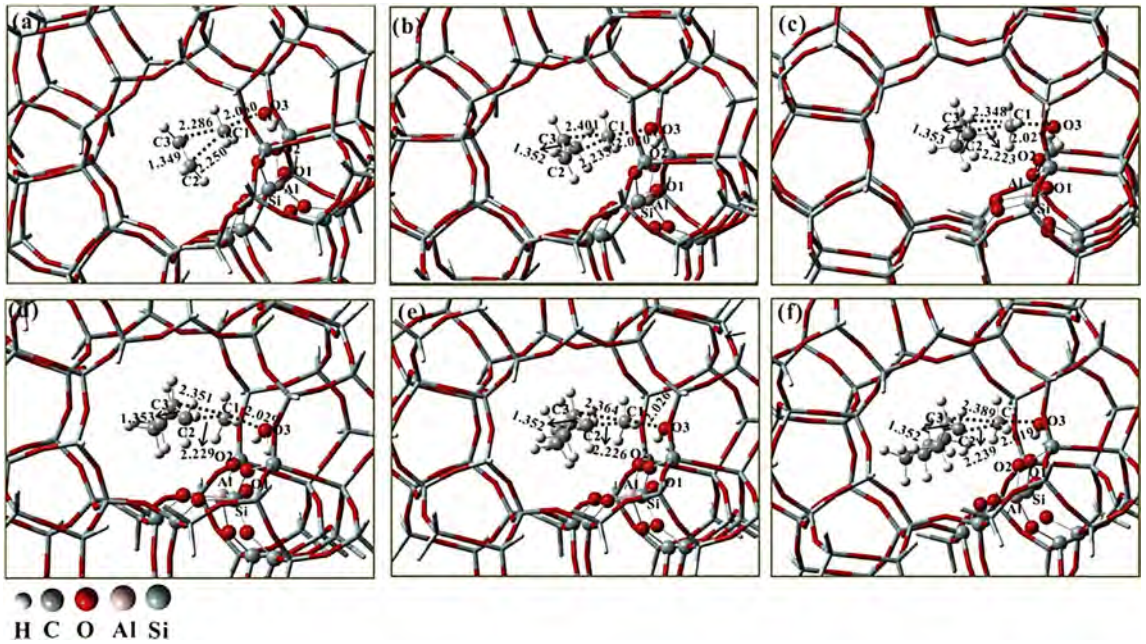

Fig. 3. Optimized structures of the olefin methylations on the Al-ZSM-5 of 72T model: (a) ethene (**Me0**) (b) propene (**Me1**) (c) butene (**Me2**) (d) pentene (**Me3**) (e) hexene (**Me4**) (f) heptene (**Me5**). Selected bond distances (in Å) are indicated.

more stable intermediates and transition states are formed caused by the additional methyl group [57].

It is apparently obtained the result from Table 1 that considering the entire zeolite framework can sharply decrease the activation barriers of methylation comparing to the reaction on the 8T model. The activation barriers are *ca.* 25.27–31.53 kcal/mol when the complete pore structure is involved, being decreased by 5.4–9.0 kcal/mol compared to 8T model (34.26–36.94 kcal/mol). It's theoretically demonstrated that the transition states can be considerably stabilized by the weak van der Waals interactions from zeolite framework of 72T model than 8T model without zeolite pore structure, thus, the reactivity of methylation on the Al-ZSM-5 of 72T model is more preferred as compared to the Al-ZSM-5 of 8T bare model. The improvement of the methylation reactivity while considering the entire zeolite pore framework was due to the stability of the formed carbenium ions derived from the confinement effect of zeolite framework.

3.1.2. Isomerization reaction

After methylation step, carbenium ions are formed that can be easily converted by isomerization reaction. Carbenium ions are considered as important intermediates in zeolite-catalyzed methanol conversion reactions [58,59], and in the isomerization reaction, the type of carbenium ions directly affects the cracking reaction [60–63]. The isomerization reactions such as methyl group shifts, H shifts and skeletal isomerization were studied on H-SAPO-34 [26], H-ZSM-5 [25] and H-ZSM-22 [52] in previous studies. In our work, H shift as the main type of isomeration reaction was calculated from C_4^+ to C_6^+ (corresponding to the alkoxide). Figs. 4 and 5 depict the structures of the transition state (TS) for the isomerization reaction on the Al-ZSM-5 of 8T and 72T models, the activation barriers and the main geometrical parameters are provided in Table 2. The isomerization reaction occurs via H1 transfer from C1 to C2 (TS, Figs. 4 and 5). As shown in the transition state structure(Fig. 4), the isomerization reaction of C_5^+ on Al-ZSM-5 of 8T model (Fig. 4b) proceeds via the increase of C1–H1(1.356 Å) bond and C2–H1(1.300 Å) bond. Corresponding to the transition state structure of isomerization reactions on 72T model (Fig. 5b), the isomerization reaction of C_5^+ occurs accompanied with lengthening C1–H1(1.419 Å) bond and C2–H1(1.252 Å) bond.

As shown in Fig. 5, the 72T model with entire zeolite framework was used to describe the influence of confinement effect from zeolite framework. The activation barriers of H shifts were 17–24 kcal/mol, which is much close to that on the H-ZSM-22 [52] (16–33 kcal/mol) and H-SAPO-34 [26] (*ca.* 1.45 ev = 33.44 kcal/mol). The isomerization reaction of H shifts need lower barriers on H-ZSM-5 that is accordance with the previous conclusion [25]. In all of the isomeration reactions, the formations of primary carbenium ion from **I1-1**, **I2-2**, and **I3-2** need higher activation barriers (20.46, 20.83, 23.73 kcal/mol) which ascribed to the unstable primary carbenium ion. The formations of second carbenium ion (**I2-1**, **I3-1**) only need activation barriers of 17.35 and 20.23 kcal/mol. It is noteworthy that the type of carbenium ions directly affects the products of the cracking reaction [60–63]. The formations of primary carbenium ion from C_4^+ to C_6^+ (**I1-1**, **I2-2**, **I3-2**) relate to the cracking reaction (**Cr1-1, Cr2-2, Cr3-3)** that generates ethene.

The similar confinement effect on the stabilities of transition states has been observed as well. For the isomerization reactions of the primary carbenium ions formation (C_4^+, C_5^+, C_6^+), the activation barriers were increased from 20.46, 20.83 and 23.73 kcal/mol on Al-ZSM-5 of 72T model to 43.29, 42.81 and 39.03 kcal/mol on Al-ZSM-5 of 8T model without zeolite framework. The other carbenium ions formations follow the same tendency when they are confined inside the zeolite framework. All the calculated activation barriers of various isomerization reactions on Al-ZSM-5 of 72T model with complete zeolite framework are lower than that on 8T model. It's suggested that the interactions between zeolite framework and adsorbed species play a key role in determining the catalytic reactivity.

3.1.3. Cracking reaction

As mentioned above, the confinement effect of zeolite framework can affect the activities of methylation and isomerization in the alkenes-based cycle. The influence of confinement effect of zeolite framework on the cracking reaction was also examined. In the reaction of cracking, β-scission is the predominant mechanism over solid acid catalysts [60–63], which occurs through protonated cyclopropyl (PCP) transition state [25,26]. The cracking reaction generates alkenes and carbenium ions. Figs. 6 and 7 provided the structures of transition state for the cracking reaction on the 8T cluster model and 72T cluster model of Al-ZSM-5. The structure of transition state indicated that the C1–C2 bond is broken with the formations of the lower carbon chain carbenium ion and light alkenes. In the case of C_5^+ cracking to propene (**Cr2-1**, Fig. 6b) catalyzed on Al-ZSM-5 of 8T model, C_2^+ and propene are generated. The bond of C1–C2 was increased from 1.529 Å of absorbed state to 2.445 Å of transition state. And the bonds of C1–C2 (2.445 Å) and C1–C3 (2.509 Å) formed the structure of protonated cyclopropyl (PCP) transition state [25,26]. Firstly, the activation barriers of producing olefins from the same carbenium ion (e.g., C_6^+) decrease gradually from ethene (E_{act} = 54.77 kcal/mol) to butene (E_{act} = 46.44 kcal/mol) catalyzed on Al-ZSM-5 of 8T model. It is evident that the formation of ethene needs higher activation barriers as compared to others, which is further confirmed that reaction involved ethene may need higher activation barriers inside the MTO alkenes-based cycle mechanism. In addition, the reactivity of the ethene formations from various primary carbenium ions such as C_4^+, C_5^+ and C_6^+ through the pathways **Cr1-1**, **Cr2-2** and **Cr3-3** (as shown in Scheme 1) have been compared. The activation barrier of ethene formation from C_4^+ (**Cr1-1**, E_{act} = 57.63 kcal/mol) to C_6^+ (**Cr3-3**, E_{act} = 54.77 kcal/mol) on the Al-ZSM-5 of 8T model is found to decrease gradually, which follows a monotonically decrease trend with the increase of carbenium ion size. It further illustrates that the transition state can be stabilized by the additional methyl group [57]. And the gradual decrease of activation barriers from the ethene formation (54.77 kcal/mol), propene formation (48.73 kcal/mol) to butene formation (46.44 kcal/mol) from C_6^+ cracking (Table 3) catalyzed by 8T Al-ZSM-5, indicated that the ethene formation needs to overcome higher barrier comparing with the propene and butene. And the calculated result is consistent with the experiment result that ethene formation from C_6^+ cracking exhibits low reaction rate and high activation barrier [62,63] than propene and butene.

The optimized structures of the transition state for cracking reaction catalyzed on the 72T model with entire zeolite framework were shown in Fig. 7, and the corresponding activation barriers were summarized in Table 3. The activation barriers of all the cracking reactions on H-ZSM-5 are 29.53–38.89 kcal/mol, which were found to be lowered than the same reactions on H-SAPO-34 (1.8–2.16 ev/42–46.3 kcal/mol) [26]. Considering the comparison of methylation and isomeration reaction on H-ZSM-5 and H-SAPO-34, the alkenes-based cycle may be easier to occur on H-ZSM-5 than H-SAPO-34. And the activation barriers of cracking reaction catalyzed on the 72T model decreased by 17.63–21.64 kcal/mol inside H-ZSM-5 channel comparing with the 8T bare model. For instance, the activation barrier for ethene generating is 38.89 (**Cr1-1**), 37.50(**Cr2-2**) and 37.14 kcal/mol (**Cr3-3**) from C_4^+, C_5^+ and C_6^+

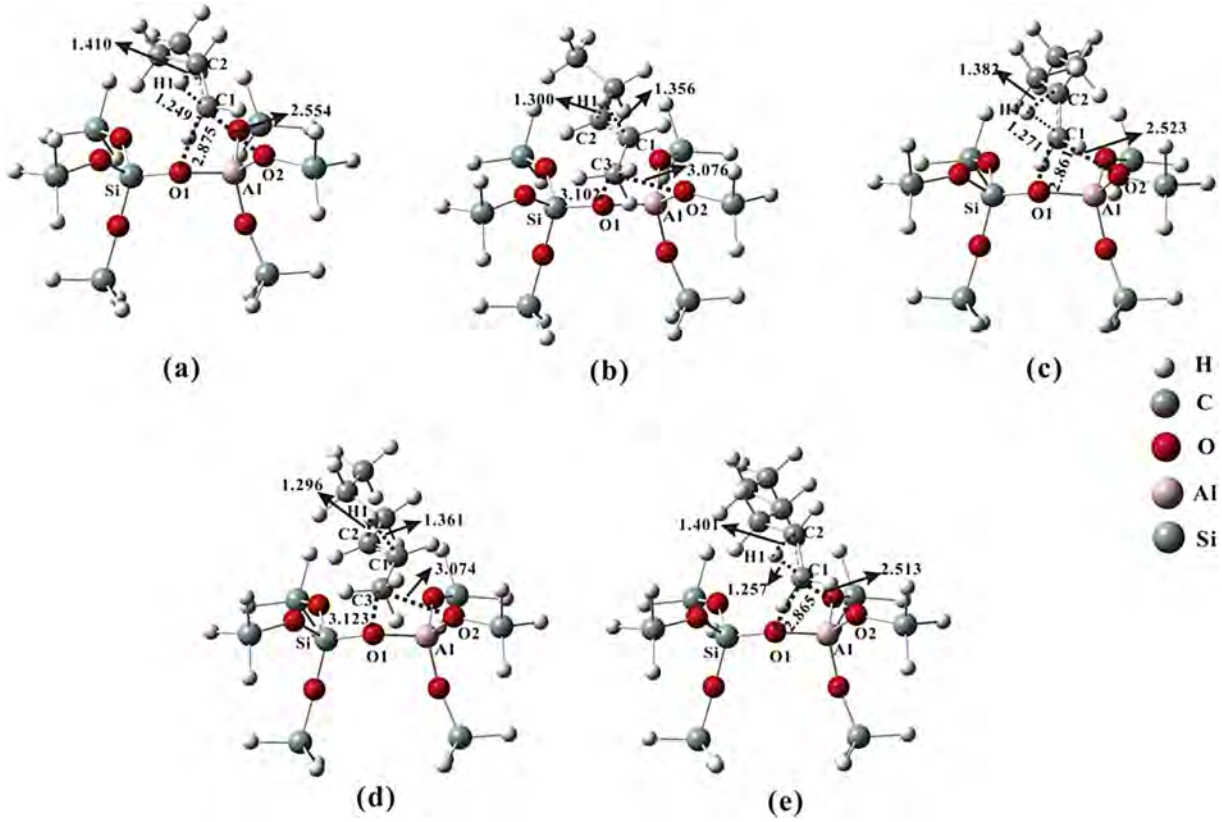

Fig. 4. Optimized geometries of the transition state (TS) for the isomerization reaction on Al-ZSM-5 of 8T model: secondary to primary carbenium ion of C_4^+ (**I1-1, a**); secondary to secondary carbenium ion of C_5^+ (**I2-1, b**) secondary to primary carbenium ion of C_5^+ (**I2-2, c**); secondary to secondary carbenium ion of C_6^+ (**I3-1, d**); secondary to primary carbenium ion of C_6^+(**I3-2, e**). Selected bond distances (in Å) are indicated.

cracking on 72T Al-ZSM-5 model that is lower than the ethene generating from C_4^+(57.63 kcal/mol), C_5^+(56.38 kcal/mol) and C_6^+(54.77 kcal/mol) cracking on 8T Al-ZSM-5 model without zeolite framework. It is suggested that the zeolite framework offers additional stabilization to the transition states resulting in improving the reactivity for cracking reaction.

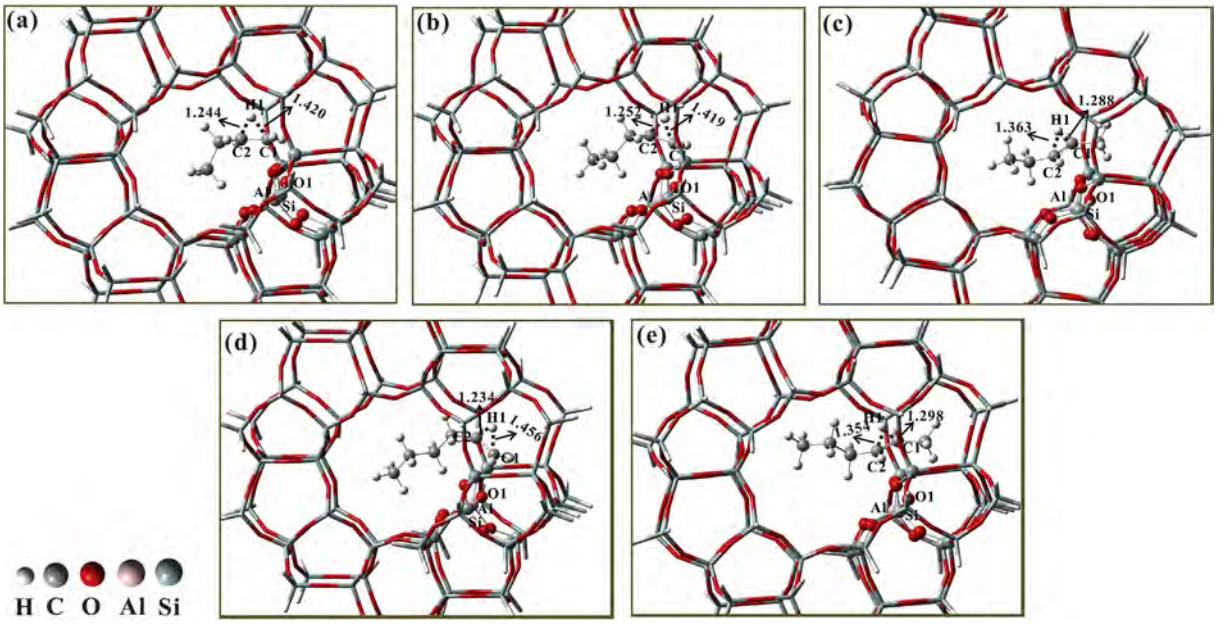

Fig. 5. Optimized structures of the isomerization reaction of carbenium ions on Al-ZSM-5 of 72T model: secondary to primary carbenium ion of C_4^+ (**I1-1, a**); secondary to secondary carbenium ion of C_5^+(**I2-1, b**) secondary to primary carbenium ion of C_5^+ (**I2-2, c**); secondary to secondary carbenium ion of C_6^+ (**I3-1, d**); secondary to primary carbenium ion of C_6^+(**I3-2, e**). Selected bond distances (in Å) are indicated.

Table 2
Activation barriers (kcal/mol) and the main geometrical parameters (Å) of transition state of the isomerization reaction of carbenium ions on the 8T Al-ZSM-5 and 72T Al-ZSM-5 cluster model: C_4^+ (**I1-1**). C_5^+ (**I2-1, I2-2**). C_6^+(**I3-1, I3-2**).

Reaction	Activation barrier		Geometry parameters (8T Al-ZSM-5)		Geometry parameters (72T Al-ZSM-5)	
	E_{8T}	E_{72T}	r_{C1-H1}	r_{C2-H1}	r_{C1-H1}	r_{C2-H1}
I1-1	43.29	20.46	1.249	1.410	1.420	1.244
I2-1	28.53	17.35	1.356	1.300	1.419	1.252
I2-2	42.81	20.83	1.271	1.382	1.288	1.363
I3-1	26.47	20.23	1.361	1.296	1.456	1.234
I3-2	39.03	23.73	1.257	1.401	1.298	1.354

In order to visualize the effect of the van der Waals (vdW) interaction on the transition state stabilities, the influence of the vdW interactions deriving from zeolite confinement on different reactions have analyzed by visualizing the isosurfaces of reduced density gradient in real space [50,51,64] as shown in Fig. 8. And Fig. 9 depicts the energy profile for the reactions (**Me2, I2-1, I2-2, Cr2-2**) from butene methylation to the cracking of $C_5H_{11}^+$ catalyzed on the 72T Al-ZSM-5 and 8T Al-ZSM-5. Taking the examples of three reactions (C_5^+ formation from butene methylation (**Me2**), C_5^+ isomerization reaction (**I2-2**) and C_5^+ cracking reaction (**Cr2-2**), Fig. 8), it is obviously seen that transition states on 72T model suffer the vdW interactions (green region as shown in Fig. 8) from the zeolite framework comparing with that of 8T model on Al-ZSM-5, which can effectively stabilize the transition states and relatively reduce the activation barriers (see Table 4). It is interesting to note that the transition states of **I2-2** and **Cr2-2** have much stronger vdW interactions than **Me2** as shown in Fig. 8. Comparing with the reaction on Al-ZSM-5 of 8T model, the activation barriers of **I2-2** and **Cr2-2** on Al-ZSM-5 of 72T model have been dramatically decreased by 21.98 and 21.64 kcal/mol than that of **Me2** (8.99 kcal/mol). This demonstrates that the zeolite confinement effect can effectively stabilize the transition states, and the relativities of isomerization and cracking reactions are more sensitive to the zeolite framework. In addition, the vdW interactions of confinement effect from entire zeolite framework can also stabilize the formed carbenium ions in the alkenes-based cycle.

3.2. Effects of acid strength on the methanol conversation following alkenes-based cycle

As discussed in the section above, the zeolite confinement effect could stabilize the transition state structures of alkenes–based cycle via vdW interactions from the zeolite framework, resulting in the high catalyzed reactivity confined in the zeolite pores. Besides the confinement effect, the acid strength of zeolite also leads great influence on reactivity and mechanism. Therefore, the influence of zeolite activity on the MTO reactivity is also explored. The models with different acid strength (Al-ZSM-5, B-ZSM-5) of the 72T models consist of the entire zeolite framework.

3.2.1. Olefin methylation

In order to explore the acid strength on the reactivity of methylation reaction, weaker acidity B-ZSM-5 was investigated theoretically, and the transition state structures are shown in Fig. 10. The geometries of the transition state for methylation step is much similar to that already described on Al-ZSM-5 (Fig. 3). The transition state structure of propene methylation on B-ZSM-5 involves the increase of the C1—O3 bond length from 1.428 Å (adsorbed state) to 2.023 Å (transition state) and the C2═C3 bond distance from 1.330 to 1.352 Å (Fig. 10b). And the activation barrier

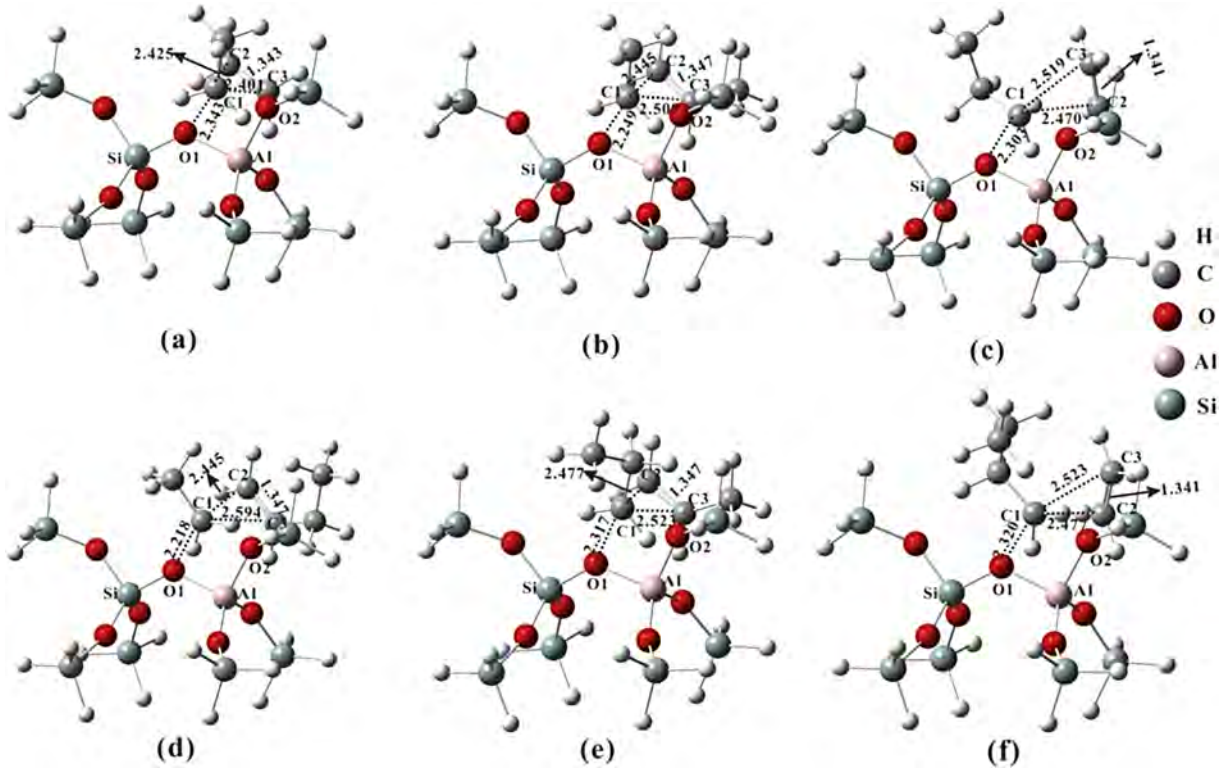

Fig. 6. Optimized geometries of the transition state (TS) for the cracking reaction on Al-ZSM-5 of 8T model: (a) C_4^+ cracking into ethene (**Cr1-1**) (b) C_5^+ cracking into propene (**Cr2-1**) (c) C_5^+ cracking into ethene (**Cr2-2**) (d) C_6^+ cracking into butene(**Cr3-1**) (e) C_6^+ cracking into propene (**Cr3-2**) (f) C_6^+ cracking into ethene (**Cr3-3**). Selected bond distances in (Å) are indicated.

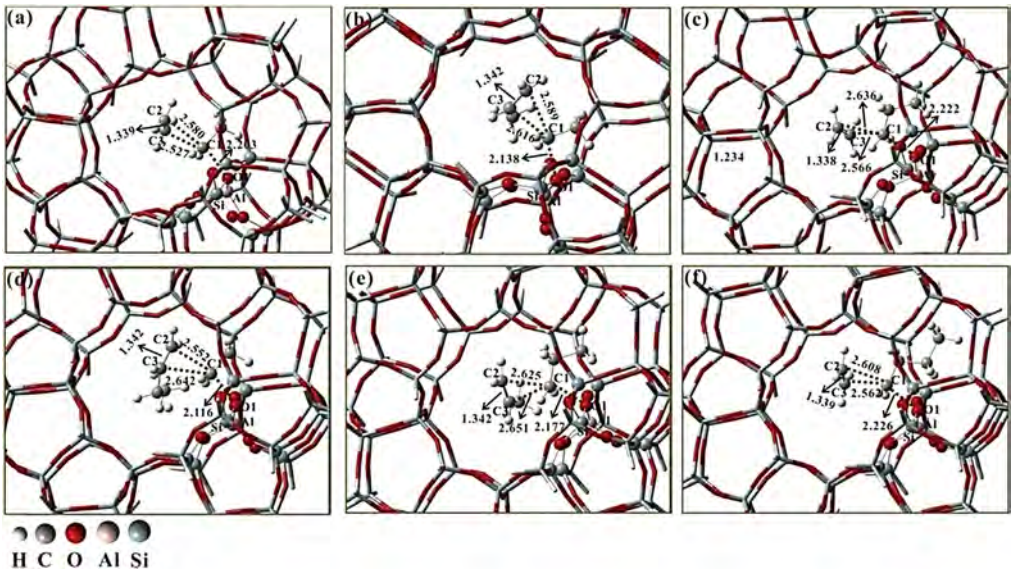

Fig. 7. Optimized structures for the cracking reaction of carbenium ions on the Al-ZSM-5 of 72T model: (a) C_4^+ cracking into ethene (**Cr1-1**) (b) C_5^+ cracking into propene (**Cr2-1**) (c) C_5^+ cracking into ethene (**Cr2-2**) (d) C_6^+ cracking into butene(**Cr3-1**) (e) C_6^+ cracking into propene (**Cr3-2**) (f) C_6^+ cracking into ethene (**Cr3-3**). Selected bond distances in (Å) are indicated.

Table 3
Activation barriers (kcal/mol) and the main geometrical parameters (Å) of the transition state of in the cracking reaction on 8T Al-ZSM-5 cluster model and 72T Al-ZSM-5 cluster model: **Cr1-1**: C_4^+ cracking into ethene. **Cr2-1**: C_5^+ cracking into propene. **Cr2-2**: C_5^+ cracking into ethene. **Cr3-1**: C_6^+ cracking into butene. **Cr3-2**: C_6^+ cracking into propene. **Cr3-3**: C_6^+ cracking into ethene.

Reaction	Activation barrier		Geometry parameters (8T Al-ZSM-5)			Geometry parameters (72T Al-ZSM-5)				
	E_{8T}	E_{72T}	r_{C1-O1}	r_{C1-C2}	r_{C1-C3}	$r_{C2=C3}$	r_{C1-O1}	r_{C1-C2}	r_{C1-C3}	$r_{C2=C3}$
Cr1-1	57.63	38.89	2.343	2.425	2.401	1.343	2.203	2.580	2.527	1.339
Cr2-1	50.34	32.03	2.249	2.445	2.509	1.347	2.138	2.589	2.616	1.342
Cr2-2	56.38	37.50	2.303	2.470	2.519	1.341	2.222	2.636	2.566	1.338
Cr3-1	46.44	29.53	2.218	2.445	2.594	1.347	2.116	2.552	2.642	1.342
Cr3-2	48.73	32.27	2.317	2.477	2.523	1.347	2.177	2.625	2.651	1.342
Cr3-3	54.77	37.14	2.320	2.477	2.523	1.341	2.226	2.608	2.562	1.339

of this process on B-ZSM-5 is computed at 29.54 kcal/mol, which is slightly higher than that catalyzed on the strong acid strength (29.27 kcal/mol). As summarized in Table 4, the activation barriers of all olefins methylation over B-ZSM-5 with weak acid strength are slightly higher only by 0.27–3 kcal/mol than that over Al-ZSM-5 with strong acid strength. This obviously reveals the acid strength can slightly promote the reaction activity of olefin methylation and have a good stability role for the formed carbenium ions. Such a result is accordance with the studies of alkenes-based cycle on the Al-ZSM-5 and B-ZSM-5 of 33T cluster model by Wang and co-workers [29]. The activation energies of butene and pentene methylation of the alkenes-based over Al-ZSM-5 were lower *ca.* 10 kJ/mol (2.4 kcal/mol) than over weak acidic B-ZSM-5 zeolite [29].

It's noteworthy that the activation barriers of olefin methylation from butene to heptene are *ca.* 29 kcal/mol catalyzed on B-ZSM-5 of 72T model, dramatically lower than that of ethene (33 kcal/mol). It is evident that the ethene need to overcome higher activation barrier in the alkenes-based cycle of the MTO reaction catalyzed by H-ZSM-5 zeolite, and this trend is in good agreement with aforementioned theoretical results on the 72T Al-ZSM-5 model and previous catalytic experiments as well [53,54,56,65].

3.2.2. Isomerization reaction

As shown in Fig. 11, the transition states structures of isomerization reaction consist of H1 transfer from C1 atom to C2 atom on B-ZSM-5 of 72T model. It can be obviously observed that the acid strength dramatically affects the stability of the transition state. For the isomerization reactions of the primary carbenium ions formation (C_4^+, C_5^+, C_6^+), the activation barriers were increased from 20.46, 20.83 and 23.73 kcal/mol on Al-ZSM-5 of 72T model to 26.66, 26.30 and 28.19 kcal/mol on B-ZSM-5 of 72T model. The other carbenium ions formations follow the same tendency when the acid strength decreases. All the calculated activation barriers of various isomerization reactions are higher by 3.61–6.20 kcal/mol on B-ZSM-5 of 72T model than those on Al-ZSM-5 of 72T model, indicating that increasing acidity can considerably improve the reactivity of isomerization reaction.

3.2.3. Cracking reaction

Fig. 12 shows the optimized geometries of the transition state of ethene, propene and butene formation from the cracking of C_4^+, C_5^+, C_6^+ on the B-ZSM-5 of 72T cluster model, and the corresponding activation barriers are shown in Table 4. The activation barriers are *ca.* 34–48 kcal/mol on the B-ZSM-5 of 72T cluster model. The activation barriers of ethene on the B-ZSM-5 of 72T cluster model need higher activation barriers (44–48 kcal/mol) and the propene formation only need activation barriers of 34–38 kcal/mol.

It is noteworthy that, regardless of the catalysts with strong acidity or weak acidity, the activation barriers of the ethene formation from higher olefins cracking are much higher than other olefins formation (see Table 4), which illustrate that the ethene

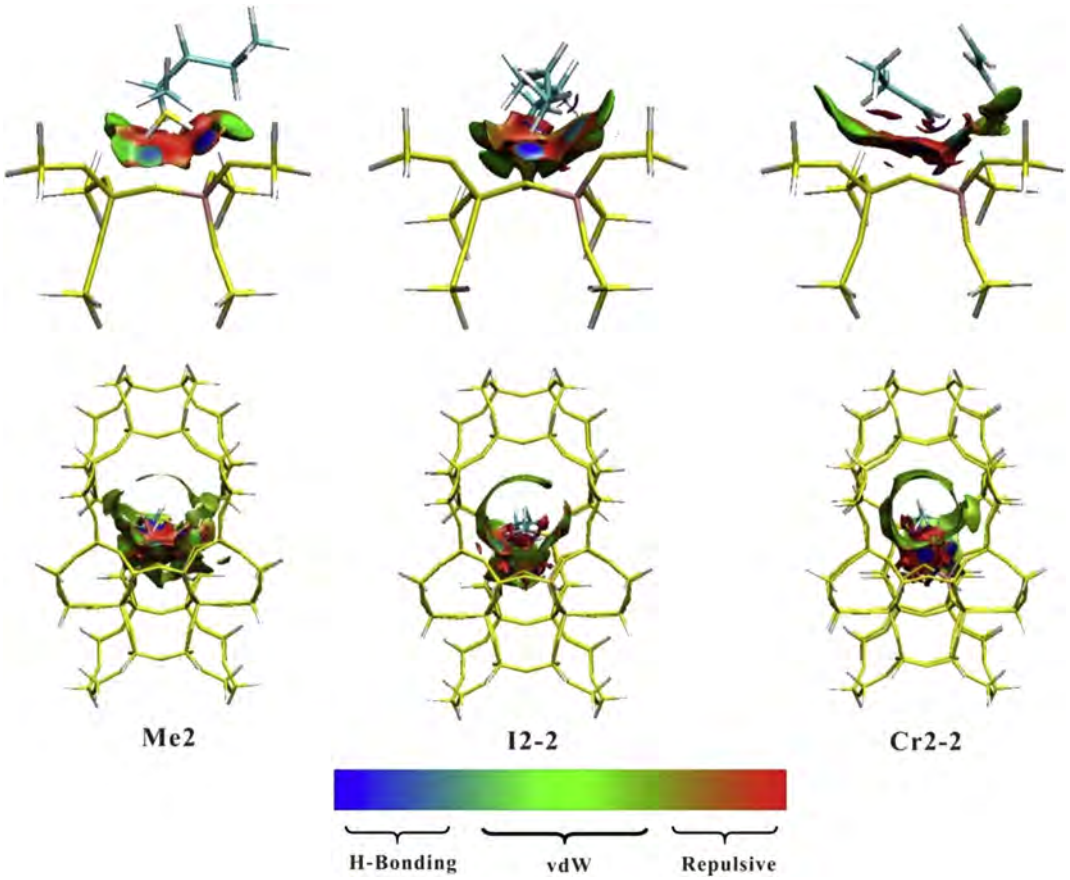

Fig. 8. Isosurface plots of reduced density gradient for the transition states species (confined in H-ZSM-5 zeolite) of C_5^+ formation from butene methylation (**Me2**), C_5^+ isomerization reaction (**I2-2**) and C_5^+ cracking to ethene (**Cr2-2**). The isosurfaces of reduced density gradient are colored according to the values of the quantity sign(λ2)ρ, and the RGB scale is indicated. vdW represents the van der Waals interaction.

formation from olefin cracking is difficult based on the alkenes-based cycle. This calculation confirmed the experiment result that the formation of ethene is different from cracking reaction of higher alkenes [15]. Moreover, combining the precursor (unstable primary carbenium ions via isomerization process described previously) of producing ethene, illustrating that the cracking reaction to ethene need higher activation barrier.

Similar to the olefin isomerization reaction, the reactivity can also be obviously improved with the acid strength increase. The influence of acid strength on the cracking reaction was also examined. For the formation of propene from C_5^+ (**Cr2-1**), the activation barrier is decreased by 3.33 kcal/mol on Al-ZSM-5(E_{act} = 32.03 kcal/mol) as compared to that on B-ZSM-5(E_{act} = 35.36 kcal/mol) with relatively weak acid strength. And

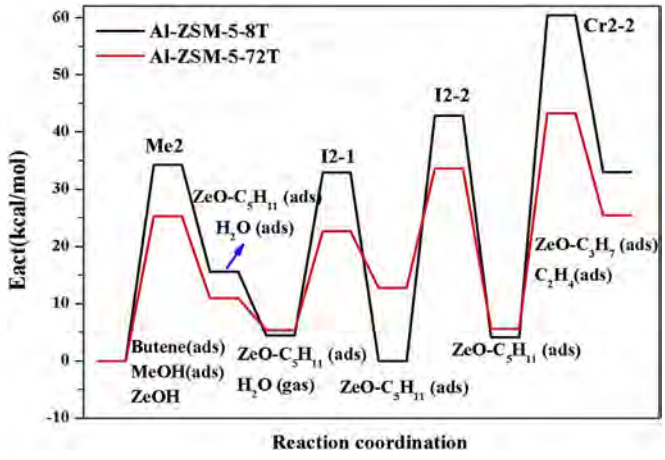

Fig. 9. Energy profiles for the reactions from butene methylation to the cracking of $C_5H_{11}^+$ catalyzed on the 72T Al-ZSM-5 and 8T Al-ZSM-5.

Table 4
Activation barriers (kcal/mol) of all the reaction route in alkenes-based cycle on different cluster models with different acid strengths and zeolite frameworks.

Reaction type[a]	Eact(kcal/mol)		
	72T-[Al]-ZSM-5	8T- [Al]-ZSM-5	72T-[B]-ZSM-5
Me0	31.53	36.94	32.98
Me1	29.27	36.47	29.54
Me2	25.27	34.26	29.26
Me3	26.61	34.72	29.21
I1-1	20.46	43.29	26.66
I2-1	17.35	28.53	20.96
I2-2	20.83	42.81	26.30
I3-1	20.23	26.47	23.90
I3-2	23.73	39.03	28.19
Cr1-1	38.89	57.63	47.72
Cr2-1	32.03	50.34	35.36
Cr2-2	37.5	56.38	44.27
Cr3-1	29.53	46.44	34.67
Cr3-2	32.27	48.73	37.65
Cr3-3	37.14	54.77	47.81

[a] The reaction type was shown in Scheme 1.

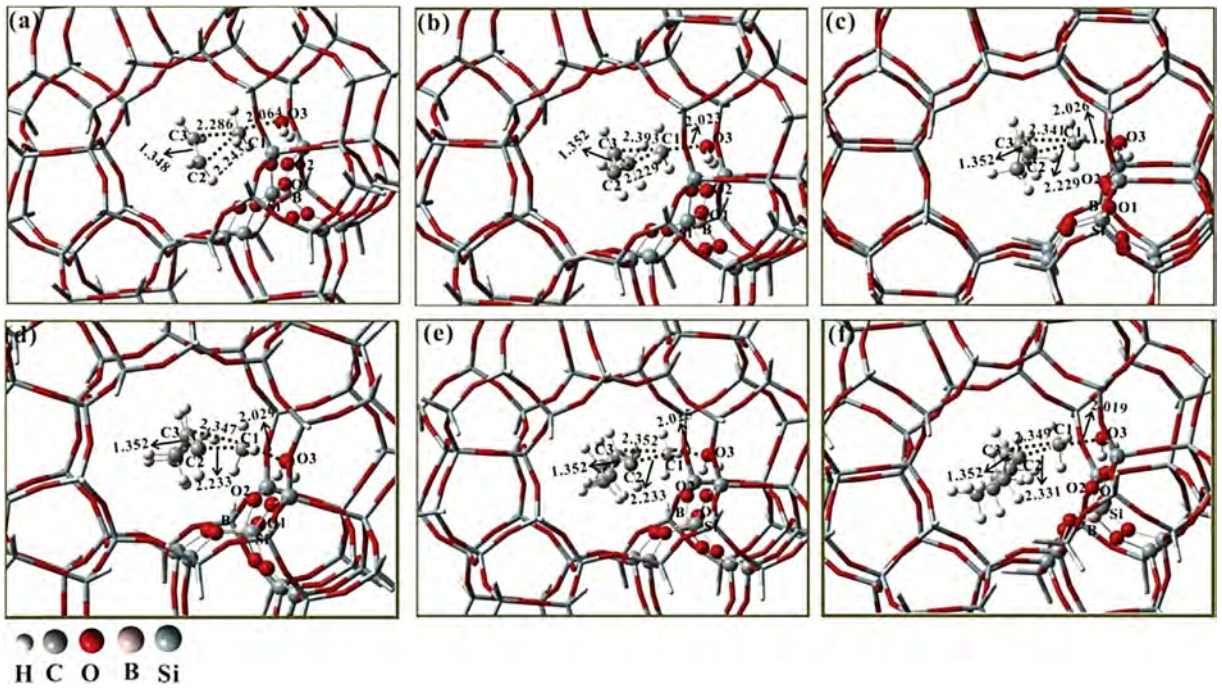

Fig. 10. Optimized geometries of the transition state (TS) for the olefin methylation on B-ZSM-5 of 72T model: (a) ethene (**Me0**) (b) propene (**Me1**) (c) butene (**Me2**) (d) pentene (**Me3**) (e) hexene (**Me4**) (f) heptene (**Me5**). Selected bond distances (in Å) are indicated.

the formation of butene from C_6^+ (**Cr3-1**), the activation barrier is lower by 5 kcal/mol on Al-ZSM-5 (29.53 kcal/mol) than that on B-ZSM-5 (34.67 kcal/mol). However, the activation barriers of the cracking reaction of ethene formation decrease by 7–10 kcal/mol, indicating increasing acid strength can strongly decrease the activation barriers of ethene formation. It is speculated that the cracking reaction of ethene formation may dominate over strong acid strength.

3.3. Effects of confinement effect and acid strength on the branched carbenium ions reactions following alkenes-based cycle

For the conversations of linear olefins and linear carbenium ions on the alkenes-based cycle reactions, the pore confinement effect and acid strength have represented great influences on the reaction activities of alkenes-based cycle. Despite of the linear olefins and carbenium ions, the isomerization of carbenium ions by H-shift,

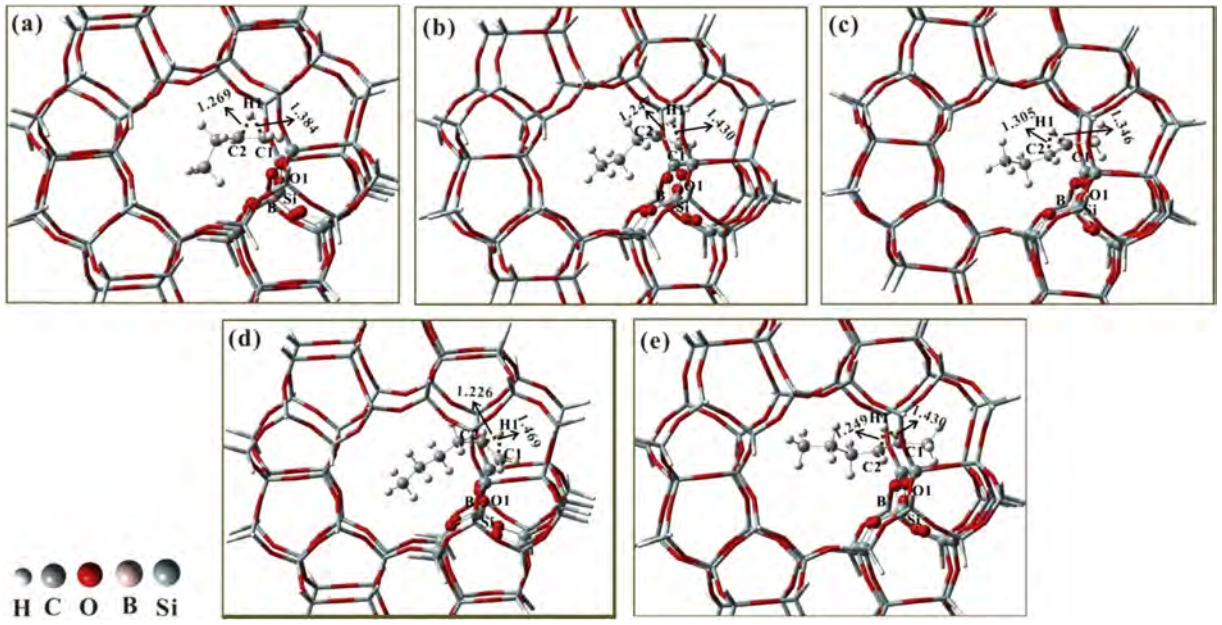

Fig. 11. Optimized structures of the transition state (TS) for the isomerization reaction of carbenium ions on B-ZSM-5 of 72T model: secondary to primary carbenium ion of C_4^+ (**I1-1, a**); secondary to secondary carbenium ion of C_5^+ (**I2-1, b**) secondary to primary carbenium ion of C_5^+ (**I2-2, c**); secondary to secondary carbenium ion of C_6^+ (**I3-1, d**); secondary to primary carbenium ion of C_6^+ (**I3-2, e**). Selected bond distances (in Å) are indicated.

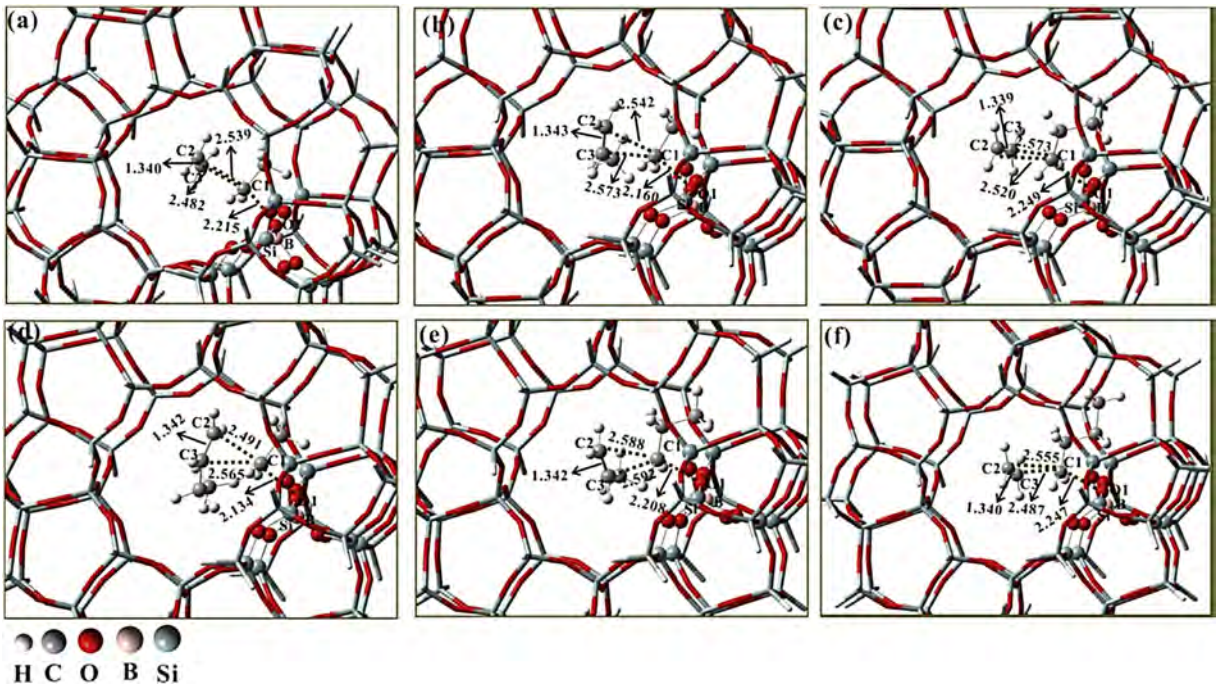

Fig. 12. Optimized geometries of the transition state (TS) for the cracking reaction of carbenium ions on B-ZSM-5 of 72T model: (a) C_4^+ cracking into ethene (**Cr1-1**) (b) C_5^+ cracking into propene (**Cr2-1**) (c) C_5^+ cracking into ethene (**Cr2-2**) (d) C_6^+ cracking into butene (**Cr3-1**) (e) C_6^+ cracking into propene (**Cr3-2**) (f) C_6^+ cracking into ethene (**Cr3-3**). Selected bond distances (in Å) are indicated.

CH_3-shift and skeletal isomerization [26] would result in the formation of other kind of olefins such as branched structures for chain propagation, therefore, the evolution of $\mathbf{C_5^+}$ species are also as an example to study the influences of the pore confinement effect and acid strength on alkenes-based cycle (as shown in Scheme 2).

Table 5 shows the activation barriers of $\mathbf{C_5^+}$ species in the alkenes-based cycle for MTO conversion on different cluster models with different acid strengths and zeolite frameworks. Similar to the reactions of the linear olefins and liner carbenium ions, it is clear to show that considering the entire zeolite framework can decrease the activation barriers of reactions comparing to the reaction on the 8T model. The activation barriers are *ca.* 9.97–43.95 kcal/mol (Table 5) when the complete pore structure is involved, being decreased by 6.4–27.05 kcal/mol compared to 8T model (14.24–56.74 kcal/mol). In addition, the branched species react more easily than the linear species. For example, the activation barriers of methylation for branched olefins such as **Me3-3**, **Me3-4** and **Me3-5** were lower by 2 kcal/mol than the linear olefin methylation (**Me3**, **Me3-1**, **Me3-2**), which is consistent with the result of previous work [25,26]. Comparing to the B-ZSM-5 (72T model), the relatively stronger acidity of Al-ZSM-5 will result in a decrease of activation barriers at 1.49–9.19 kcal/mol. It is confirmed that increasing acid strength and considering pore confinement effect could decrease the activation barriers and improve reaction activity for all of the reactions in alkenes-based cycle.

4. Conclusions

The key roles of pore confinement effect and acid strength on the alkenes-based cycle have been established by density functional theory calculations. It's demonstrated the catalytic reactivity can be effectively enhanced by stabilizing of the transition states

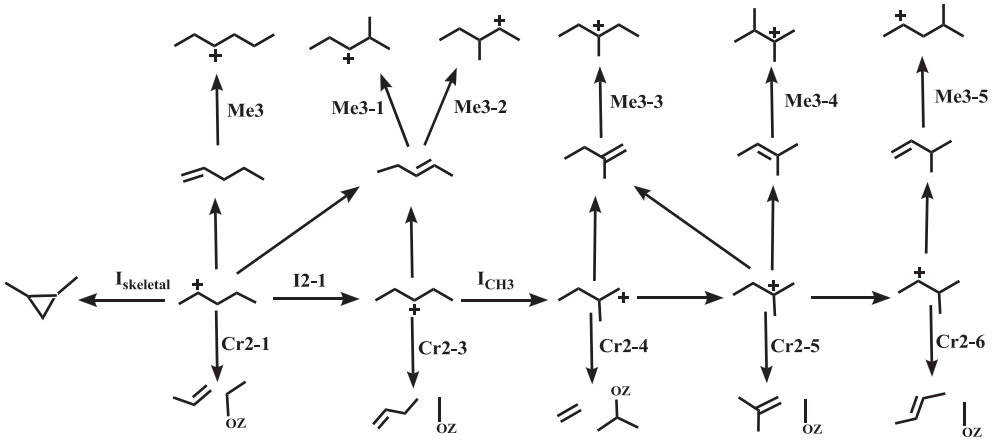

Scheme 2. Evolution of $\mathbf{C_5^+}$ species in the alkenes-based cycle for MTO conversion.

Table 5
Activation barriers (kcal/mol) of C_5^+ species in the alkenes-based cycle for MTO conversion on different cluster models with different acid strengths and zeolite frameworks.

Reaction type[a]	Eact (kcal/mol)		
	72T-[Al]-ZSM-5	8T- [Al]-ZSM-5	72T-[B]-ZSM-5
Me3	26.61	34.72	29.21
Me3-1	25.27	33.22	27.70
Me3-2	25.17	33.22	27.71
Me3-3	24.30	32.92	27.34
Me3-4	24.14	31.44	27.19
Me3-5	27.22	34.25	28.71
$\mathbf{I_{skeletal}}$	19.47	25.82	22.43
$\mathbf{I_{CH3}}$	22.70	35.36	27.48
I2-1	9.97	32.96	14.24
Cr2-1	32.03	50.34	35.36
Cr2-3	43.95	56.74	47.49
Cr2-4	33.02	51.89	38.28
Cr2-5	35.71	42.11	35.68
Cr2-6	21.44	48.49	30.63

[a] The reaction type was shown in Scheme 2.

with the zeolite framework. From the visualized isosurface plots of reduced density gradient, it was clearly illustrated that the transition states can be considerably stabilized by the weak van der Waals interactions from zeolite framework. On the other hand, the theoretical results have also confirmed that acid strength increase can significantly improve the catalytic reactivity of all steps (i.e., olefin methylation, isomerization and cracking), as proved by the decrease of activation barriers.

Furthermore, the catalytic processes involving ethene present relatively higher activation barriers than the other olefins regardless the catalyst used, implying less reactivity. In addition, increasing acid strength can largely decrease the activation barrier of ethene formation of cracking reaction, illustrating that the ethene formation of cracking reaction may dominate over strong acid strength. Our work will provide assistance for understanding the mechanism of MTO reaction and optimizing zeolite catalysts and reaction condition of methanol to olefins.

Acknowledgements

We are grateful for the financial support of the National Natural Science Foundation of China (No. 91545104, 21473182, 21522310, 21273005, and 21273230) and the Youth Innovation Promotion Association of the Chinese Academy of Sciences.

References

[1] U. Olsbye, S. Svelle, M. Bjorgen, P. Beato, T.V. Janssens, F. Joensen, S. Bordiga, K.P. Lillerud, Angew. Chem. Int. Ed. 51 (2012) 5810–5831.
[2] M. Stocker, Microporous Mesoporous Mater. 29 (1999) 3–48.
[3] A.J. Silvestri, C.D. Chang, J. Catal. 47 (1977) 249–259.
[4] I.M. Dahl, S. Kolboe, Catal. Lett. 20 (1993) 329–336.
[5] I.M. Dahl, S. Kolboe, J. Catal. 149 (1994) 458–464.
[6] S. Kolboe, I.M. Dahl, Stud. Surf. Sci. Catal. 94 (1995) 427–434.
[7] I.M. Dahl, S. Kolboe, J. Catal. 161 (1996) 304–309.
[8] a) G.A. Olah, Pure Appl. Chem. 53 (1981) 201–207;
b) G.J. Hutchings, F. Gottschalk, M.V. Michéle, R. Hunter, J. Chem. Soc. Faraday Trans. 83 (1987) 571–583;
c) Y. Ono, T. Mori, J. Chem. Soc. Faraday Trans. 77 (1981) 2209–2221;
d) D. Kagi, J. Catal. 69 (1981) 242;
e) W. Zatorski, S. Kryzanowski, Acta Phys. Chem. 29 (1978) 347;
f) J.K.A. Clarke, R. Darcy, B.F. Hegarty, E. O'Donoghue, V. Amir-Ebrahimi, J.J. Rooney, J. Chem. Soc. Chem. Commun. 5 (1986) 425–426.
[9] S.R. Blaszkowski, R.A. vanSanten, J. Am. Chem. Soc. 119 (1997) 5020–5027.
[10] D.M. Marcus, K.A. McLachlan, M.A. Wildman, J.O. Ehresmann, P.W. Kletnieks, J.F. Haw, Angew. Chem. Int. Ed. 45 (2006) 3133–3136.
[11] D. Lesthaeghe, V. Van Speybroeck, G.B. Marin, M. Waroquier, Angew. Chem. Int. Ed. 45 (2006) 1714–1719.
[12] B. Arstad, J.B. Nicholas, J.F. Haw, J. Am. Chem. Soc. 126 (2004) 2991–3001.
[13] J.B. Nicholas, J.F. Haw, J. Am. Chem. Soc. 120 (1998) 11804–11805.
[14] W. Song, J.F. Haw, J.B. Nicholas, C.S. Heneghan, J. Am. Chem. Soc. 122 (2000) 10726–10727.
[15] S. Svelle, F. Joensen, J. Nerlov, U. Olsbye, K.P. Lillerud, S. Kolboe, M. Bjorgen, J. Am. Chem. Soc. 128 (2006) 14770–14771.
[16] M. Bjorgen, S. Svelle, F. Joensen, J. Nerlov, S. Kolboe, F. Bonino, L. Palumbo, S. Bordiga, U. Olsbye, J. Catal. 249 (2007) 195–207.
[17] C. Wang, Y. Wang, H. Liu, G. Yang, Y. Du, Z. Xie, Chin. J. Catal. 36 (2015) 1573–1579.
[18] S. Xu, A. Zheng, Y. Wei, J. Chen, J. Li, Y. Chu, M. Zhang, Q. Wang, Y. Zhou, J. Wang, F. Deng, Z. Liu, Angew. Chem. Int. Ed. 52 (2013) 11564–11568.
[19] J. Li, Y. Wei, J. Chen, P. Tian, X. Su, S. Xu, Y. Qi, Q. Wang, Y. Zhou, Y. He, Z. Liu, J. Am. Chem. Soc. 134 (2012) 836–839.
[20] J. Wang, Y. Wei, J. Li, S. Xu, W. Zhang, Y. He, J. Chen, M. Zhang, A. Zheng, F. Deng, X. Guo, Z. Liu, Catal. Sci. Technol. 6 (2016) 89–97.
[21] C. Wang, J. Xu, G. Qi, Y. Gong, W. Wang, P. Gao, Q. Wang, N. Feng, X. Liu, F. Deng, J. Catal. 332 (2015) 127–137.
[22] C. Wang, Y. Chu, A. Zheng, J. Xu, Q. Wang, P. Gao, G. Qi, Y. Gong, F. Deng, Chem. Eur. J. 20 (2014) 12432–12443.
[23] R.M. Dessau, R.B. Lapierre, J. Catal. 78 (1982) 136–141.
[24] R.M. Dessau, J. Catal. 99 (1986) 111–116.
[25] D. Lesthaeghe, J. Van der Mynsbrugge, M. Vandichel, M. Waroquier, V. Van Speybroeck, ChemCatChem 3 (2011) 208–212.
[26] C. Wang, Y. Wang, Z. Xie, J. Catal. 301 (2013) 8–19.
[27] C. Wang, Y. Wang, Z. Xie, Catal. Sci. Technol. 4 (2014) 2631–2638.
[28] C. Wang, Y. Wang, Y. Du, G. Yang, Z. Xie, Catal. Sci. Technol. 5 (2015) 4354–4364.
[29] S. Wang, Y. Chen, Z. Wei, Z. Qin, H. Ma, M. Dong, J. Li, W. Fan, J. Wang, J. Phys. Chem. C 119 (2015) 28482–28498.
[30] K.Y. Lee, S.W. Lee, S.K. Ihm, Ind. Eng. Chem. Res. 53 (2014) 10072–10079.
[31] Y. Chu, B. Han, A. Zheng, F. Deng, J. Phys. Chem. C 116 (2012) 12687–12695.
[32] L. Lin, C. Qiu, Z. Zhuo, D. Zhang, S. Zhao, H. Wu, Y. Liu, M. He, J. Catal. 309 (2014) 136–145.
[33] D. Lesthaeghe, B. De Sterck, V. Van Speybroeck, G.B. Marin, M. Waroquier, Angew. Chem. Int. Ed. 46 (2007) 1311–1314.
[34] E. Lalik, X.S. Liu, J. Klinowski, J. Phys. Chem. C 96 (1992) 805–809.
[35] C.T.W. Chu, C.D. Chang, J. Phys. Chem. C 89 (1985) 1569–1571.
[36] J. Wang, J. Li, S. Xu, Y. Zhi, Y. Wei, Y. He, J. Chen, M. Zhang, Q. Wang, W. Zhang, X. Wu, X. Guo, Z. Liu, Chin. J. Catal. 36 (2015) 1392–1402.
[37] C. Wang, R.Y. Brogaard, Z.K. Xie, F. Studt, Catal. Sci. Technol. 5 (2015) 2814–2820.
[38] Y. Chu, B. Han, H. Fang, A. Zheng, F. Deng, Microporous Mesoporous Mater. 151 (2012) 241–249.
[39] E. Gianotti, M. Manzoli, M.E. Potter, V.N. Shetti, D. Sun, J. Paterson, T.M. Mezza, A. Levy, R. Raja, Chem. Sci. 5 (2014) 1810.
[40] Y. Chu, P. Ji, X. Yi, S. Li, P. Wu, A. Zheng, F. Deng, Catal. Sci. Technol. 5 (2015) 3675–3681.
[41] H. Vankoningsveld, H. Vanbekkum, J.C. Jansen, Acta Crystallogr. 43 (1987) 127–132.
[42] C.T.-W. Chu, G.H. Kuehl, R.M. Lago, C.D. Chang, J. Catal. 93 (1985) 451–458.
[43] A.J. Jones, R.T. Carr, S.I. Zones, E. Iglesia, J. Catal. 312 (2014) 58–68.
[44] J.D. Padraig, J. O'Malley, Zeolites 8 (1988) 317–321.
[45] L.A. Clark, M. Sierka, J. Sauer, J. Am. Chem. Soc. 126 (2004) 936–947.
[46] D.K. Papayannis, K.D. Papavasileiou, V.S. Melissas, Microporous Mesoporous Mater. 226 (2016) 1–9.
[47] J.D. Chai, M. Head-Gordon, Phys. Chem. Chem. Phys. 10 (2008) 6615–6620.
[48] G.W. Trucks, M.J. Frisch, H.B. Schlegel, G.E. Scuseria, J.R. Cheeeseman, M.A. Robb, G. Scalmani, V. Barone, B. Mennucci, H. Nakatsuji, G.A. Petersson, M. Caricato, X. Li, H.P. Hratchian, J. Bloino, A.F. Izmaylov, G. Zheng, J.L. Sonnenberg, M. Hada, K. Toyota, M. Ehara, R. Fukuda, J. Hasegawa, M. Ishida, T. Nakajima, O. Kitao, Y. Honda, H. Naka, T. Vreven, J.A. Montgomery, F. Ogliaro, J.E. Peralta, M. Bearpark, J.J. Heyd, E. Brothers, K.N. Kudin, R. Kobayashi, V.N Staroverov, J. Normand, K. Raghavachari, J.C. Burant, A. Rendell, S.S. Iyengar, J. Tomasi, M. Cossi, N. Rega, M. Klene, J.M. Millam, J.E. Knox, J.B. Cross, V. Bakken, J. Jaramillo, C. Adamo, R. Gomperts, R.E. Stratmann, O. Yazyev, R. Cammi, A.J. Austin, C. Pomelli, J.W. Ochterski, R.L. Martin, V.G. Zakrzewski, K. Morokuma, G.A. Voth, P. Salvador, S. Dapprich, J.J. Dannenberg, A.D. Daniels, O. Farkas, J.V. Ortiz, J.B. Foresman, J. Cioslowski, D.J. Fox, Gaussian 09, Revision B.01, 2010. Wallingford, CT.
[49] C.-Y. Sung, S. Al Hashimi, A. McCormick, M. Cococcioni, M. Tsapatsis, Microporous Mesoporous Mater. 172 (2013) 7–12.
[50] E.R. Johnson, S. Keinan, P. Mori-Sanchez, J. Contreras-Garcia, A.J. Cohen, W. Yang, J. Am. Chem. Soc. 132 (2010) 6498–6506.
[51] T. Lu, F. Chen, J. Comput. Chem. 33 (2012) 580–592.
[52] Y. Chu, X. Sun, X. Yi, L. Ding, A. Zheng, F. Deng, Catal. Sci. Technol. 5 (2015) 3507–3517.
[53] S. Svelle, P.O. Rønning, S. Kolboe, J. Catal. 224 (2004) 115–123.
[54] S. Svelle, P. Ronning, U. Olsbye, S. Kolboe, J. Catal. 234 (2005) 385–400.
[55] S. Svelle, C. Tuma, X. Rozanska, T. Kerber, J. Sauer, J. Am. Chem. Soc. 131 (2009) 816–825.
[56] I.M. Hill, Y.S. Ng, A. Bhan, ACS Catal. 2 (2012) 1742–1748.
[57] I.M. Hill, S. Al Hashimi, A. Bhan, J. Catal. 285 (2012) 115–123.
[58] N. Rosenbach, A.P.A. dos Santos, M. Franco, C.J.A. Mota, Chem. Phys. Lett. 485 (2010) 124–128.

[59] M.V. Frash, V.B. Kazansky, A.M. Rigby, R.A. vanSanten, J. Phys. Chem. B 101 (1997) 5346–5351.
[60] J. Abbot, B.W. Wojciechowski, Can. J. Chem. Eng. 63 (1985) 462–469.
[61] A. Corma, A.V. Orchilles, Microporous Mesoporous Mater. 35–36 (2000) 21–30.
[62] C.-J. Chen, S. Rangarajan, I.M. Hill, A. Bhan, ACS Catal. 4 (2014) 2319–2327.
[63] J.S. Buchanan, J.G. Santiesteban, W.O. Haag, J. Catal. 158 (1996) 279–287.
[64] W. Sun, R. Di Felice, J. Phys. Chem. C 116 (2012) 24954–24961.
[65] I.M. Hill, S.A. Hashimi, A. Bhan, J. Catal. 291 (2012) 155–157.